Radio Science, Volume 30, Number 5, Pages 1499–1510, September–October 1995

Parameterized ionospheric model: A global ionospheric parameterization based on first principles models

R. E. Daniell, Jr.,[1] L. D. Brown,[1] D. N. Anderson,[2] M. W. Fox,[3]
P. H. Doherty,[4] D. T. Decker,[4] J. J. Sojka,[5] and R. W. Schunk[5]

Abstract. We describe a parameterized ionospheric model (PIM), a global model of theoretical ionospheric climatology based on diurnally reproducible runs of four physics based numerical models of the ionosphere. The four numerical models, taken together, cover the *E* and *F* layers for all latitudes, longitudes, and local times. PIM consists of a semianalytic representation of diurnally reproducible runs of these models for low, moderate, and high levels of both solar and geomagnetic activity and for June and December solstice and March equinox conditions. PIM produces output in several user selectable formats including global or regional latitude/longitude grids (in either geographic or geomagnetic coordinates), a set of user-specified points (which could lie along a satellite orbital path), or an altitude/azimuth/elevation grid for a user-specified location. The user selectable output variables include profile parameters (f_oF_2, h_mF_2, total electron content, etc.), electron density profiles, and ion composition (O^+, NO^+, and O_2^+).

1. Introduction

For the past 7 years, we have been developing a real-time ionospheric specification model for the Air Force Air Weather Service (AFAWS) for use at the Air Force Space Forecast Center (AFSFC, also known as the 50th Weather Squadron). This model, PRISM (Parameterized Real-time Ionospheric Specification Model) uses both ground based and space based data to update a climatological model in near real time. The climatological model, a parameterized ionospheric model known as PIM, is a composite of diurnally reproducible runs of several physical ionospheric models: (1) the time dependent ionospheric model (TDIM) of Utah State University (USU) [*Schunk*, 1988], (2) the low latitude F region model (LOWLAT) developed by *Anderson* [1973], (3) the midlatitude version of LOWLAT (called MIDLAT) developed by D. N. Anderson and modified by D. T. Decker, and (4) an E region local chemistry code (ECSD) developed by D. T. Decker and incorporating photoelectrons using the continuous slowing down method [*Jasperse*, 1982]. Thus unlike previous empirical models (such as the International Reference Ionosphere, IRI) that are based on empirical climatology, PIM is based on theoretical climatology.

We have made PIM available to the ionospheric community on an informal basis for several years, and the feedback from PIM users has resulted in substantial improvements. The purpose of this paper is to provide a description of PIM and to make it generally available to interested users. PRISM will be made available to the ionospheric research community through the AFAWS and will be described in a future publication.

PIM can produce output in three formats: (1) gridded output on a regional or global grid in geographic or geomagnetic latitude and longitude, (2) output at a set of user specified points in either geographic or geomagnetic coordinates, and (3) output on a grid of altitude, azimuth, and elevation from a user specified

[1]Computational Physics, Incorporated, Waltham, Massachusetts.
[2]Geophysics Directorate, Phillips Laboratory, Hanscom Air Force Base, Massachusetts.
[3]Center for Space Physics, Boston University, Boston, Massachusetts.
[4]Institute for Space Research, Boston College, Chestnut Hill, Massachusetts.
[5]Center for Atmospheric and Space Science, Utah State University, Logan.

Paper number 95RS01826.
0048-6604/95/95RS-01826$08.00

point. The second option may be used to specify output along a satellite orbital track, but the output is at fixed UT. The output data is of two types: electron density and ion composition profiles, and profile parameters (f_oF_2, h_mF_2, total electron content (TEC), etc.). The user may select either type or both.

Our primary objective in the development of PIM was to produce a convenient summary of the output of physics-based numerical models for a variety of geophysical conditions ("theoretical climatology"). We believe that for many applications this approach has significant advantages over empirical models. First, empirical models are limited by the amount and kind of available data. For example, the original CCIR coefficients [*International Radio Consultative Committee (CCIR)*, 1967] were obtained from monthly median values of f_oF_2 during 1954-1958 from approximately 150 ionosondes around the world. Since these ionosondes were sparsely distributed in ocean areas and in the southern hemisphere, the resulting maps of f_oF_2 were of limited value in those regions. *Rush et al.* [1983, 1984] improved the maps by supplementing the data with theoretical calculations using LOWLAT. The result was an improved set of coefficients [*Fox and McNamara*, 1988], generally known as the URSI-88 coefficient set [*Rush et al.*, 1989]. However, these coefficients are based on monthly median values organized in terms of solar activity [low and high]. As *Klobuchar and Doherty* [1992] have demonstrated, the daily variation of the ionosphere (especially the F region) is poorly correlated with the daily variation of solar activity as tracked by indices such as $F_{10.7}$ or sunspot number. This is probably due to the large daily variability of thermospheric winds, which in turn is due partly to daily variations in geomagnetic activity and partly to daily variability of gravity wave sources in the lower atmosphere. The net result is that empirical models average data over very different ionospheric conditions corresponding to the same solar activity level. Thus ionospheric features that move around on a daily basis will be smeared out or broadened and reduced in amplitude. Any empirical model which does not organize the data in terms of all of the driving forces that govern the ionosphere will have this property.

The principle distinction between empirical climatology and theoretical climatology may be stated as follows:

Empirical climatology yields an "average" ionosphere in which the average may be taken over very different ionospheric configurations. Persistent features such as the subauroral trough, auroral oval, or equatorial anomaly may be smeared out or broadened as a result of the averaging process. Empirical climatology is limited by the amount of data and the spatial and temporal distribution of that data.

Theoretical climatology yields a "representative" ionosphere, i.e., an ionosphere that corresponds to a potentially realizable set of specific geophysical conditions. Ionospheric features will have locations, widths, amplitudes similar to those that might be observed on any given day under the specified geophysical conditions. Theoretical climatology is limited by the accuracy and completeness of the physics and chemistry included in the theoretical models on which it is based and the computer resources required to span the full range of geophysical conditions.

For many purposes, the average ionosphere of an empirical model is all that is required. However, many users have the need to simulate the performance of an operational system under representative conditions. For those users, a representative ionosphere is more useful than an average ionosphere. PIM was designed for just this purpose.

2. The Physical Models

Four separate physical models were used as the basis of PIM: (1) a low-latitude F layer model (LOWLAT), (2) a midlatitude F layer model (MIDLAT), (3) a combined low and middle latitude E layer model (ECSD), and (4) a high-latitude E and F layer model (TDIM). All four models are based on a tilted dipole representation of the geomagnetic field and a corresponding geomagnetic coordinate system. (Hereafter, "latitude" means "geomagnetic latitude" unless otherwise noted.) All four models use the MSIS-86 neutral atmosphere model [*Hedin*, 1987]. Chemical reaction rates, collision frequencies, and similar data are consistent among all the models.

2.1. The Low-Latitude *F* Layer Model

The low latitude F region model (LOWLAT) was originally developed by *Anderson* [1973]. (See also *Moffett* [1979]). It solves the diffusion equation for O^+ along a magnetic flux tube. Normally, the entire flux tube is calculated with chemical equilibrium boundary conditions at both feet of the flux tube. A large number of flux tubes must be calculated in order to build up an altitude profile.

Since heat transport is not included in this model, ion and electron temperature models must be used. For the PRISM development effort we chose the temperature model of *Brace and Theis* [1981] with altitude interpolation based on the analytic forms of *Strobel and McElroy* [1970]. The Horizontal Wind Model (HWM) of *Hedin* [1988] was used to describe thermospheric winds. (Most of the model runs were made well before the latest version [*Hedin*, 1994] became available.)

The critical feature incorporated in the low-latitude model is the dynamo electric field. The horizontal component of this field drives upward convection through **E×B** drift, and this can significantly modify profile shapes and densities. This phenomenon is responsible for the equatorial anomaly, crests in ionization on either side of the magnetic equator at ±15–20° magnetic latitude. In the current version of PIM (version 1.3) the **E×B** driven vertical drift used for these calculations was based on the empirical models derived from data from the Atmospheric Explorer-E (AE-E) satellite [*Fejer et al.*, 1995], which are consistent with the drifts measured at Jicamarca [*Fejer*, 1981; *Fejer et al.*, 1989] but include longitudinal variations as well. We used the *Fejer et al.* [1995] empirical drifts for high solar activity. Following their discussion, we modified these drifts by reducing or eliminating the prereversal enhancement for moderate or low solar activity. In all cases, the published drift model was modified to ensure no net vertical motion after 24 hours, as is necessary for diurnally reproducible runs. Horizontal drifts were neglected in the PRISM runs.

Since its original development this model has undergone extensive validation by comparison with data. The most recent such comparison is by *Preble et al.* [1994], who used electron density profiles measured by the incoherent scatter radar facility at Jicamarca, Peru.

2.2. The Midlatitude F Layer Model

The midlatitude *F* region model (MIDLAT) is the same as the low latitude version except that the dynamo electric field is not included. Complete flux tubes are followed, but neither horizontal nor vertical convection is included. The computer resource requirements of MIDLAT are far less than those of LOWLAT. As long as the boundary between low and middle latitudes is chosen so that the electric field is negligible on the boundary flux tubes, the two models give identical results at the boundary, ensuring continuity across that boundary. For the PRISM development effort we used the same temperature model [*Brace and Theis*, 1981] and the same thermospheric wind model [*Hedin*, 1988]. For appropriate production, loss, and diffusion rates for both LOWLAT and MIDLAT, see *Decker et al.* [1994].

2.3. The Low and Midlatitude E Layer Model

The low- and midlatitude *E* region model (ECSD) was developed by D. T. Decker and J. R. Jasperse and incorporates photoelectrons calculated using the continuous slowing down (CSD) approximation [*Jasperse*, 1982]. Ion concentrations are calculated assuming local chemical equilibrium. A small nighttime source is included to ensure that an *E* layer is maintained throughout the night.

2.4. The High Latitude Model

The high latitude model (incorporating both *E* and *F* layers) is the Utah State University (USU) time dependent ionospheric model (TDIM). (See *Schunk* [1988] for a review.) This model is similar to the low- and midlatitude models except that the flux tubes are truncated and a flux boundary condition is applied at the top. In addition, the flux tubes move under the influence of the high latitude convection electric field. In the low latitudes, because the magnetic field is mainly horizontal, the effect of the electric field is primarily to move the ionization in altitude. In contrast, the high-latitude magnetic field is mainly vertical, and the electric field driven convection is horizontal. Like LOWLAT, this model has a long history and has been validated by numerous comparisons with data [e.g., *Sojka et al.*, 1994].

TDIM includes an *E* layer model that incorporates the effects of ionization by precipitating auroral particles. The ion production rates used were calculated using the B3C electron transport code [*Strickland et al.*, 1976, 1994] and incident electron spectra representative of DMSP SSJ/5 data. The characteristics of the electron spectra were taken from the *Hardy et al.* [1987] electron precipitation model. The high-latitude convection patterns were those developed by *Heppner and Maynard* [1987] for southward directed B_z. Until high-latitude convection under northward B_z is better understood, we suggest using PIM with low *Kp* for B_z north conditions.

3. Parameterization of the Physical Models

Parameterization of the physical models proceeded in two steps. First, the models were used to generate a number of "databases" for a discrete set of geophysical

conditions. Each database consists of ion density profiles on a discrete grid of latitudes and longitudes for a 24-hour period in UT. Second, to reduce storage requirements, the databases were approximated with semianalytic functions. These two processes are described in the following subsections.

3.1. Geophysical Parameters

All the physical models were parameterized in terms of season and solar activity. The mid- and high-latitude models were also parameterized in terms of magnetic activity, while the high latitude model was additionally parameterized in terms of the sign of the interplanetary magnetic field component B_y. (The high-latitude model was only run using B_z southward. Northward B_z conditions are modeled using the low magnetic activity databases.) For the middle and low latitudes, the F layer (O^+) and the E layer (NO^+ and O_2^+) were computed and parameterized separately. The high-latitude model (TDIM) produced all three ions simultaneously.

Due to time and computer resource limitations, only a few values of each parameter were used. The season "values" are the June and December solstices and the March equinox (which also stands in for the September equinox). We expect to change from seasonal to monthly values in the next major version of PIM. The values of the other parameters are summarized for each latitude region in Table 1. Note that the USU TDIM and LOWLAT models produce output in magnetic local time (MLT), while MIDLAT and ECSD produce output in magnetic longitude.

3.2. Representation of the Databases

When the models are run for any one set of geophysical parameters (e.g., June, $F_{10.7}$ = 130, Kp = 1), they produce ion densities (O^+, NO^+, and O_2^+) on a four-dimensional grid. MIDLAT and ECSD use a grid of magnetic latitude (λ), magnetic longitude (φ), altitude (z), and universal time (τ). TDIM uses magnetic local time (MLT or ψ) instead of magnetic longitude, while LOWLAT uses MLT instead of UT. In order to make this mass of numbers more manageable, we produced a semianalytical representation of each database. The space and time grid parameters are summarized for each latitude region in Table 2.

Because of the computer resource requirements of the low latitude F layer code, it was used to generate databases at four discrete longitudes (corresponding to longitude sectors for which E×B drift measurements were available). Each longitude sector was parameterized separately, and the necessary longitude interpolation is carried out in PIM and PRISM during execution, as described below.

Because we were trying to represent discrete data (rather than continuous functions), and because we were working with regional rather than global data sets, we felt that the usual spherical harmonic expansion techniques were not appropriate. Instead we concentrated on the use of orthogonal functions of discrete variables.

We first considered the use of modified Chapman functions for representing altitude profiles of ion densities. These functions have the advantage that peak height and peak density are explicit parameters, but the

Table 1. Geophysical Parameter Values

	Solar Activity, $F_{10.7}$	Magnetic Activity, Kp	IMF B_y Direction	Number of databases
Low Latitude F layer	70, 130, 210	N/A	N/A	36[a]
Midlatitude F layer	70, 130, 210	1, 3.5, 6	N/A	54[b]
Low & Midlatitude E layer	70, 130, 210	1, 3.5, 6	N/A	54[c]
High Latitude E & F layer	70, 130, 210	1, 3.5, 6	+, -	324[d]

N/A, not applicable.

[a]Three seasons times three solar activities times four longitude sectors.

[b]Three seasons times three solar activities times three magnetic activities times two hemispheres.

[c]Three seasons times three solar activities times three magnetic activities times two species.

[d]Three seasons times three solar activities times three magnetic activities times two B_y's times three species times two hemispheres.

Table 2. Horizontal Grid Parameters

Latitude Region	Magnetic Latitude	Magnetic Longitude	UT	Altitude Profiles per Database
Low-latitude *F* layer	−32° to 32° in 2° steps	80°, 180°, 260°, and 320°	MLT: 0.0 to 23.5 in 0.5 hour steps	1,584
Midlatitude *F* layer	30° to 74° and −30° to −74° in 4° steps	0° to 345° in 15° steps	0100 to 2300 in 2 hour steps	3,456
Low- and midlatitude *E* layer	−76° to 76° in 4° steps	0° to 345° in 15° steps	0100 to 2300 in 2 hour steps	11,232
High-latitude *E* and *F* layer	51° to 89° and −51° to −89° in 2° steps	MLT: 0.5 to 23.5 in 1 hour steps	0100 to 2300 in 2 hour steps	5,760

extremely nonlinear nature of these functions necessitates the use of nonlinear least squares fitting methods. While such methods produced excellent representations of individual profiles, the variation of the fitted parameters with latitude, longitude (or MLT), and UT was unacceptably noisy. Consequently, we chose to use empirical orthonormal functions for the altitude representation.

Empirical orthonormal functions (EOFs) have been used extensively to represent meteorological and climatological data [*Lorenz*, 1956; *Kutzbach*, 1967; *Davis*, 1976; *Peixoto and Oort*, 1991]. They have also been used for empirical ionospheric modeling [*Secan and Tascione*, 1984] (EOFs are described in Appendix A). They have the advantage of providing a representation in terms of linear combinations of orthogonal functions, which allows for straightforward determination of coefficients. However, because peak density and peak height are not explicit parameters of the representation, these parameters can be determined only by reconstructing the entire profile and invoking a peak-finding algorithm. We expect to revisit this problem in future versions of PIM and PRISM and implement a new representation that combines the attractive features of both methods, that is, that includes peak density and peak height as explicit parameters yet relies on linear combinations of orthogonal functions to describe the profile shape.

For longitude (or local time) variations (and for the low-latitude *F* layer UT variation), the obvious choice is a Fourier series, since trigonometric functions retain their orthogonality properties on uniform discrete grids and because the data is periodic in the independent variable. These worked quite well for the high-latitude models under all conditions and for the low- and midlatitude models under low to moderate solar activity conditions. However, they did not work well for the low- and midlatitude models under high solar activity

Table 3. Notation Summary

Grid	Variable	Variable Index	Orthogonal Function	Function Index
Altitude	z_i	$1 \le i \le I$	EOF: $g_m(z_i)$	$1 \le m \le M$
Latitude	λ_j	$1 \le j \le J$	polynomial: $u_n(\lambda)$	$0 \le n \le N$
Longitude	φ_k	$1 \le k \le K$	not used	
MLT	ψ_k, ψ_l	$1 \le k \le K$, $1 \le l \le L$	TDIM: $a_{mp}^{(s)}(\lambda_j,\tau_l)\cos(p\psi)+b_{mp}^{(s)}(\lambda_j,\tau_l)\sin(p\psi)$ all others: not used	$0 \le p \le P$
UT	τ_l	$1 \le l \le L$	not used	

conditions, apparently because the EOF coefficients exhibited exceptionally large gradients at dawn and dusk. Therefore we decided to tabulate the coefficients in longitude for all the low- and midlatitude databases.

For the latitude variations we chose to generate grid-specific orthogonal polynomials using the algorithm derived by *Beckmann* [1973] and described in Appendix B. To help keep the notation straight, we summarize it in Table 3.

The semianalytic representation of each database was generated in several steps. For all ionospheric regions the first step was the determination of the EOFs from the ion densities in the database and a set of coefficients $c_{lm}(\lambda_j,\varphi_k)$ for representing each ion density profile on the latitude, longitude, UT grid (see Appendix A).

TDIM:

$$n_s(z_i,\lambda_j,\psi_k,\tau_l) \approx \sum_{m=1}^{M} c_m^{(s)}(\lambda_j,\psi_k,\tau_l) g_m^{(s)}(z_i) \quad (1a)$$

MIDLAT, ECSD:

$$n_s(z_i,\lambda_j,\varphi_k,\tau_l) \approx \sum_{m=1}^{M} c_m^{(s)}(\lambda_j,\varphi_k,\tau_l) g_m^{(s)}(z_i) \quad (1b)$$

LOWLAT:

$$n_s(z_i,\lambda_j,\varphi_k,\psi_l) \approx \sum_{m=1}^{M} c_m^{(s)}(\lambda_j,\varphi_k,\psi_l) g_m^{(s)}(z_i) \quad (1c)$$

where z_i, λ_j, φ_k, ψ_k, τ_j, and ψ_l are all points on the model output grid, and $g_m^{(s)}(z_i)$ is the m^{th} EOF evaluated at z_i. (Note, however, that a different set of $g_m^{(s)}(z_i)$ functions are used for each ion, for each set of geophysical conditions, and for each model.)

For the high latitude model (TDIM, both *E*- and *F*-layers), the second step was the generation of Fourier coefficients in MLT, $a_{mp}^{(s)}(\lambda_j,\tau_l)$ and $b_{mp}^{(s)}(\lambda_j,\tau_l)$, for each point on the latitude, UT grid.

TDIM:

$$n_s(z_i,\lambda_j,\psi,\tau_l) \approx \sum_{m=1}^{M}\sum_{p=0}^{P}\left\{a_{mp}^{(s)}(\lambda_j,\tau_l)\cos(p\psi) + b_{mp}^{(s)}(\lambda_j,\tau_l)\sin(p\psi)\right\} g_m^{(s)}(z_i) \quad (2)$$

For the low- and midlatitude models, we found that a truncated Fourier series often introduced spurious longitudinal dependences, apparently driven by the steep gradients at dawn and dusk. The effect was particularly pronounced at high solar activity when the day/night contrast is the greatest. Consequently, for these models the EOF coefficients remain tabulated in longitude.

For all models the next step was the generation of orthogonal polynomials from the latitude grid (Appendix B). For the high latitude model (TDIM) the coefficients are $\alpha_{mnp}^{(s)}(\tau_l)$ and $\beta_{mnp}^{(s)}(\tau_l)$, and the ion density is approximated by

TDIM:

$$n_s(z_i,\lambda,\psi,\tau_l) \approx \sum_{m=1}^{M}\sum_{n=0}^{N}\sum_{p=0}^{P}\left\{\alpha_{mnp}^{(s)}(\tau_l)\cos(p\psi) + \beta_{mnp}^{(s)}(\tau_l)\sin(p\psi)\right\} g_m(z_i) u_n(\lambda) \quad (3a)$$

Table 4. Altitude Grids and Emperical Orthonormal Functions

Database	Altitude Points	Minimum Altitude (km)	Maximum Altitude (km)	EOFs
Low-latitude O^+	55	160	1600	9
Midlatitude O^+	49	125	1600	8
Low- and midlatitude NO^+ and O_2^+	28	90	400	7
High-latitude O^+, NO^+, & O_2^+	37	100	800	6

Note that in none of these cases was the altitude spacing uniform.

For MIDLAT and ECSD the coefficients are $\gamma_{mn}^{(s)}(\lambda_k,\tau_l)$ and the ion density is approximated by

MIDLAT, ECSD:

$$n_s(z_i,\lambda,\varphi_k,\tau_l) \approx \sum_{m=1}^{M}\sum_{n=0}^{N}\gamma_{mn}^{(s)}(\varphi_k,\tau_l)g_m(z_i)u_n(\lambda) \quad (3b)$$

For LOWLAT the coefficients are $\eta_{mn}^{(s)}(\varphi_k,\psi_l)$ and the ion density is approximated by

LOWLAT:

$$n_s(z_i,\lambda,\varphi_k,\psi_l) \approx \sum_{m=1}^{M}\sum_{n=0}^{N}\eta_{mn}^{(s)}(\varphi_k,\psi_l)g_m(z_i)u_n(\lambda) \quad (3c)$$

The number of terms in each series are listed in Table 4 for each region.

Because of the extensive use of tabulated coefficients, the ion density at an arbitrary point must be obtained by interpolation. In PIM and PRISM, altitude interpolation is quadratic, while UT interpolation is linear. For the MIDLAT databases, the longitude interpolation is also linear, as is the local time interpolation in the LOWLAT databases. However, the longitude interpolation in the LOWLAT databases is more complicated. First, the O^+ profile for the desired magnetic latitude and local time is reconstructed for each of the four longitude sectors. Then the peak height and peak density is determined for each profile. The peak height for the desired longitude is determined by Fourier interpolation, and all four profiles are shifted to match the interpolated peak height. Then Fourier interpolation is used again at each altitude to obtain the interpolated ion density profile.

3.3 Merging the Regional Models

Because we used four different regional models in the development of PRISM, the models must be merged at region boundaries. Specifically, the low latitude and midlatitude O^+ models have to be merged across the boundary between low and middle latitudes, while all three ions (O^+, NO^+, and O_2^+) must be merged across the boundary between midlatitudes and high latitudes.

The transition from low latitude O^+ profiles to midlatitude O^+ profiles takes place between 30° and 34° in both hemispheres. The transition is accomplished by

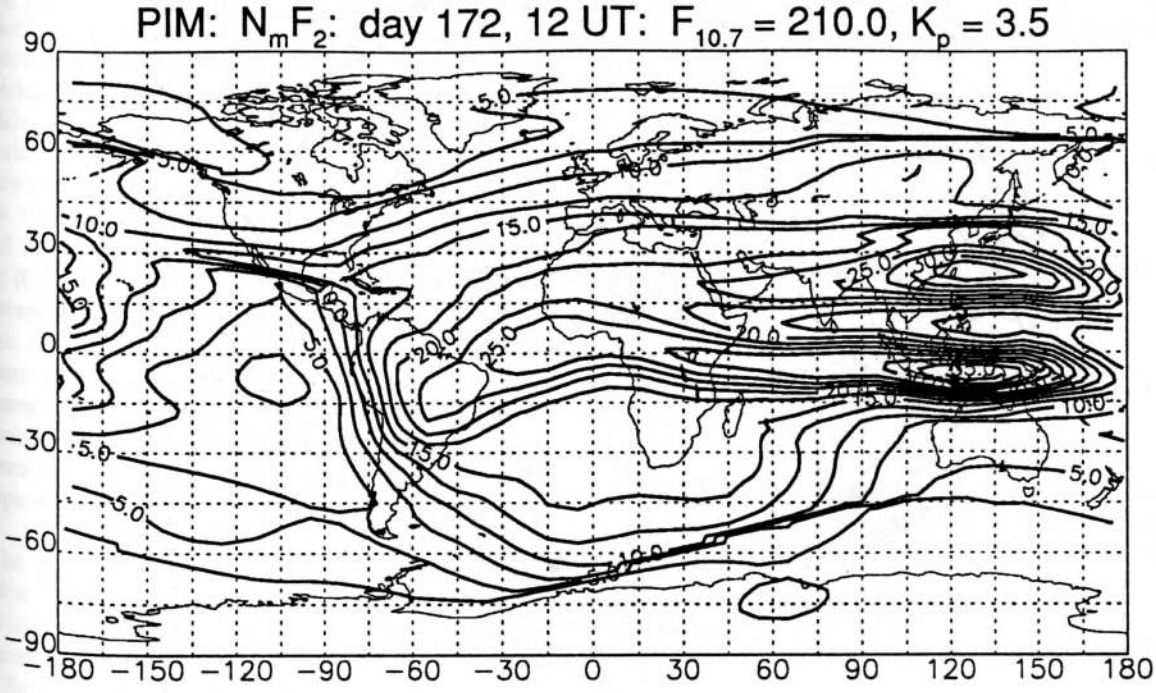

Figure 1. Contours of N_mF_2 (in units of 10^5 cm^{-3}) in cylindrical equidistant projection from PIM for high solar activity, moderate magnetic activity, at 1200 UT near the June solstice. The equatorial anomaly is clearly evident from about 1400 to 2400 local time.

taking a weighted average of the h_mF_2 values from the two models in which the weight shifts linearly from 100% low latitude at 30° to 100% midlatitude at 34°. The profiles are shifted to match the averaged h_mF_2 values and then a similar weighted average of the shifted profiles is taken to produce the final merged profile. No transition for NO^+ and O_2^+ is necessary since a single model was used for these ions.

The transition from midlatitude to high latitude takes place over an 8° wide zone extending from 50° to 58°. The transition process is similar to the low to midlatitude transition, except that the high-latitude profiles are shifted to match the h_mF_2 and h_mE values given by the midlatitude models. The final profile is produced by a weighted average of midlatitude and (shifted) high latitude profiles.

Although PIM and PRISM use geomagnetic coordinates internally, they can produce output in either geomagnetic or geographic coordinates. The conversion from geomagnetic coordinates to geographic coordinates is made using corrected geomagnetic (CGM) coordinates. Although this is not entirely consistent with the dipole coordinates used in the physical models, it does result in a more realistic representation of magnetically controlled features when presented in geographic coordinates. A contour map of N_mF_2 in geographic coordinates (cylindrical projection) for the June solstice at high solar activity and moderate magnetic activity is displayed in Figure 1. The equatorial anomaly is clearly visible between geographic longitudes 30°E and 180°E, corresponding to local times of 1400 and 2400. The high latitude is more clearly seen

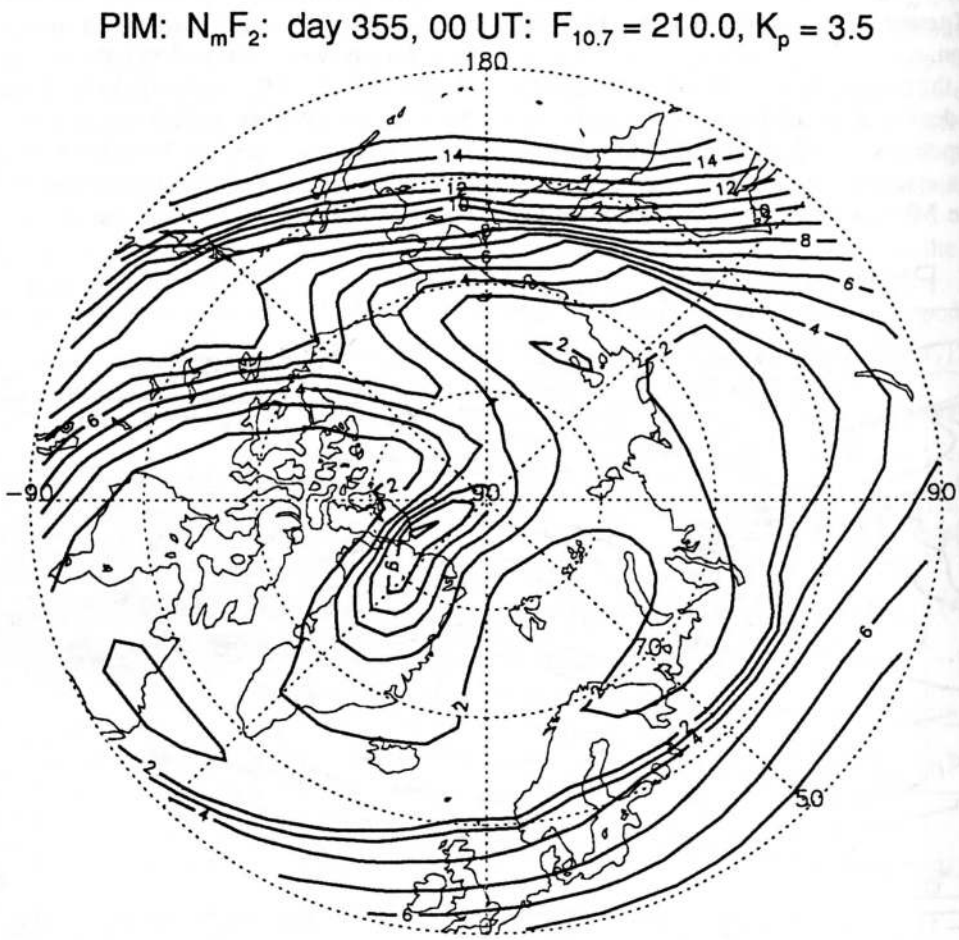

Figure 2. Contours of N_mF_2 (in units of 10^5 cm^{-3}) in polar projection from PIM for the same conditions as Figure 1 except for 0000 UT and December solstice. The "tongue of ionization" produced by a steady convection pattern is clearly evident. Local midnight is at the bottom.

in a polar projection such as is displayed in Figure 2, again in geographic coordinates. The figure shows the northern hemisphere at the December solstice. B_y is positive, and the tongue of ionization resulting from a steady convection pattern is clearly visible on the evening side.

4. Discussion

We have described PIM, a global ionospheric model based on theoretical climatology in the form of diurnally reproducible runs of a set of physics based, numerical ionospheric models. This model has been distributed to about 60 users around the world and is now available to the ionospheric community over the Internet. (Those interested in obtaining PIM should contact L. D. Brown, R. E. Daniell, or D. N. Anderson for more information.) For many users, the principal advantage of PIM over empirical models will be the more realistic representation of low- and high-latitude ionospheric features.

A number of compromises were required in the development of PIM. First, of course, was the necessity of using parameterizations (in the form of diurnally reproducible runs) of the physical models, rather than the physical models themselves. Second, we had to use empirical models (e.g., MSIS-86) instead of physical models to provide the necessary inputs to the ionospheric models. Third, we had to use a tilted dipole representation of the Earth's magnetic field instead of a more realistic model. This last compromise is mitigated somewhat by the use of the corrected geomagnetic (CGM) coordinate system to convert from internal geomagnetic coordinates to geographic coordinates. While not fully self-consistent, this does allow a more realistic representation of geomagnetically controlled features such as the equatorial anomaly. A fourth compromise was the use of only three seasons. We expect to remove these compromises one by one as available computing power increases in the future.

The particular features described here apply to PIM version 1.3. Significant enhancements to PIM are planned for the near future. H^+ ion densities based on a parameterization of the plasmasphere model of *Bailey and Sellek* [1990] will be added so that PIM can give electron density profiles up to the plasmapause. At the same time the coefficient files will be regenerated using a single global ionospheric model, eliminating the need to merge models across region boundaries. Monthly coefficients (instead of seasonal) coefficients will also be used. The analytic representations will also be reexamined in order to produce a more accurate, more efficient, and fully analytic fit to the model runs. The resulting version of PIM should be even more useful to the ionospheric community than the current version.

Appendix A Empirical Orthonormal Functions

This treatment of empirical orthogonal functions (EOFs) is based on the appendix of *Secan and Tascione* [1984], which was based on work by *Lorenz* [1956], *Kutzbach* [1967], and *Davis* [1976]. See also *Peixota and Oort* [1991]. The reader is referred to these references for mathematical proofs of the assertions made below. In the following discussion we use the notation given in Table 3.

A database consists of altitude profiles at certain longitudes, certain latitudes, and certain universal times. (See Tables 1-4.) Let S be the number of altitude profiles in a database, and let I be the number of points in each altitude profile. We would like to represent each altitude profile of the quantity Ψ (e.g., O^+concentration) as an expansion in orthogonal functions, $g_m(z_i)$:

$$\Psi_s(z_i) = \sum_{m=1}^{M} \alpha_{sm} g_m(z_i) + r_s(z_i), \qquad s = 1...S,\ i = 1...I \tag{A1}$$

where $r_s(z_i)$ is the residual, and the coefficients α_{sm} are calculated from

$$\alpha_{sm} = \sum_{i=1}^{I} \Psi_s(z_i) g_m(z_i) \tag{A2}$$

In principle, any orthogonal set of functions may be used. However, the references cited above provide an algorithm for finding the set which minimizes the RMS error for a given number of terms, $M \le I$. We summarize the algorithm here.

First define the $I \times I$ covariance matrix **C** with elements

$$C_{ij} = \frac{1}{S} \sum_{s=1}^{S} \Psi_s(z_i) \Psi_s(z_j), \qquad i, j = 1,2,...I \tag{A4}$$

Now consider the eigenvalue/eigenvector problem $C\varphi = \varphi L$ or

$$\sum_{j=1}^{I} C_{ij}\varphi_{jk} = \sum_{j=1}^{I} \varphi_{ij}\delta_{jk}\lambda_k = \varphi_{ik}\lambda_k \qquad (A5)$$

where $\varphi = \{\varphi_{ij}\}$ is the matrix of eigenvectors of $C = \{C_{ij}\}$, and $L = \{\delta_{ij}\lambda_j\}$ is a diagonal matrix whose elements are the corresponding eigenvalues. (The k^{th} column of φ is the eigenvector corresponding to the k^{th} eigenvalue, λ_k.) By convention, the eigenvectors and eigenvalues are ordered so that $\lambda_1 > \lambda_2 > \ldots > \lambda_I$. Because C is a real symmetric matrix, eigenvectors corresponding to unique eigenvalues are guaranteed to be orthogonal [e.g., *Hildebrand*, 1965]. Because of the origin of the matrix C, it is unlikely that any of its eigenvalues will be degenerate, so we may assume that φ is an orthogonal set. According to *Secan and Tascione*

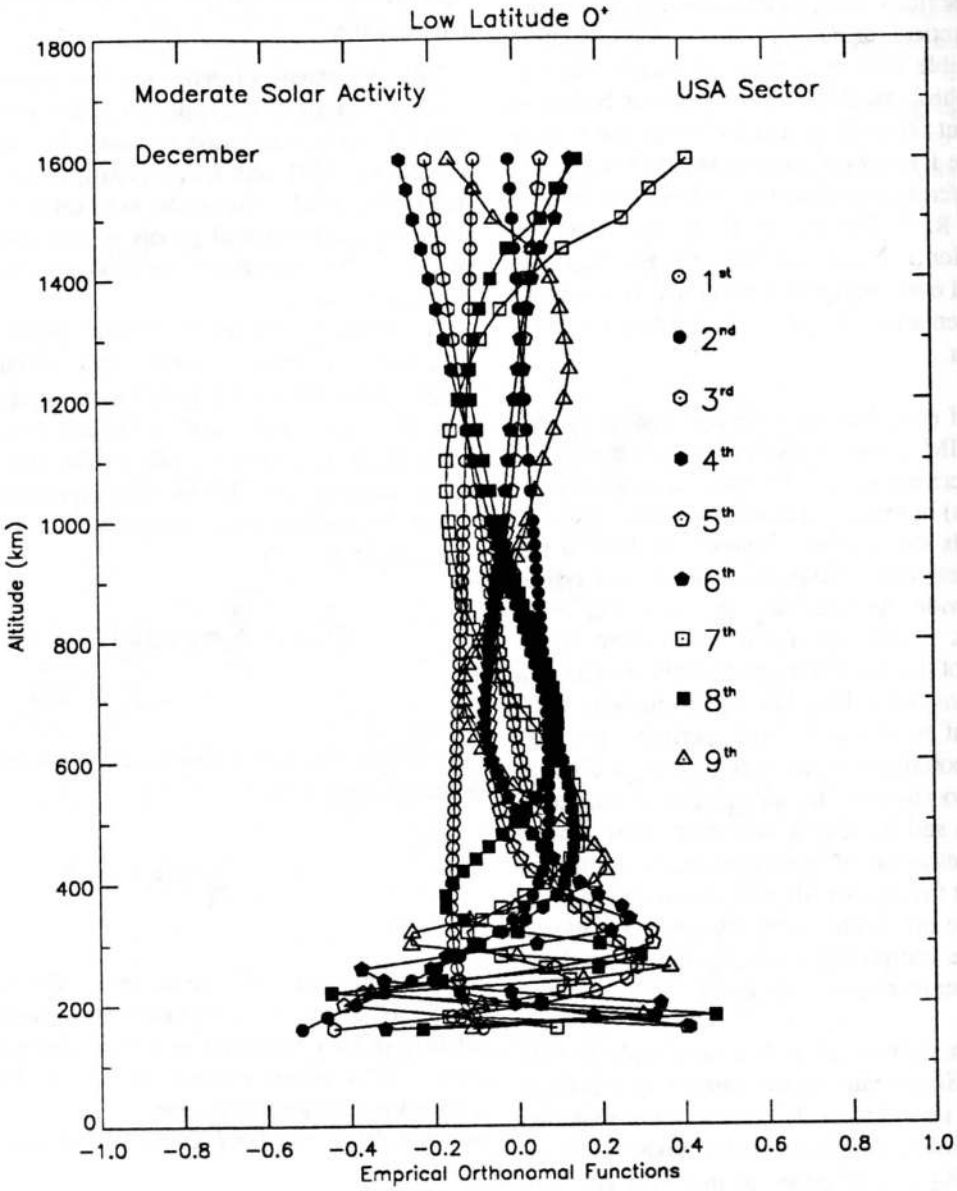

Figure A1. The empirical orthonormal functions (EOFs) for low latitude O^+ derived from the LOWLAT output databases for the American longitude sector, December solstice, moderate magnetic activity, and moderate solar activity. Only the first nine EOF's are plotted because these are the ones used in PIM.

[1984] and references therein, the set of orthogonal functions that minimizes the RMS error for M terms is just the first M eigenvectors:

$$g_m(z_i) = \varphi_{im}, \qquad i = 1,2,\ldots I;\ m = 1,2,\ldots M \qquad \text{(A6)}$$

These are the EOFs.

As a practical matter, we have found that the number of EOFs needed to provide a reasonably good representation for all the profiles is about $I/6$, as illustrated in Table 4. The only exception is the low- and midlatitude E layer (NO^+ and O_2^+), probably because these databases covered both hemispheres simultaneously. We have also found that substantial improvement in representation does not occur until the number of EOFs is about $I/2$. Furthermore, the EOFs derived for one database were inadequate for any other database, and the EOFs simultaneously derived from several databases produce noticeably poorer representations than those derived for each database individually. Consequently, we have derived separate EOF sets for each database.

The first nine EOF's derived from the low latitude F region (O^+) database for the US longitude sector, the December solstice, and moderate solar activity, are shown in Figure A1. The first EOF always has the least structure, and successive EOF's become progressively more structured. Although differing in detail, the EOF's for the other databases are qualitatively similar.

Appendix B Orthogonal Polynomials of Discrete Variables

Because the databases for which we desire analytic approximations have discrete latitude grids, we preferred to use polynomials whose orthogonality is defined in terms of that grid, rather than in terms of integrals over the interval. The algorithm for generating orthogonal polynomials on a specified grid is given by *Beckmann* [1973]. Let us denote the desired polynomials by $u_n(\lambda)$ and define $u_{-1}(\lambda) \equiv 0$ and $u_0(\lambda) \equiv 1$. Note that the polynomials are continuous functions of the continuous variable λ even though their orthogonality is defined in terms of the discrete grid $\{\lambda_j, j = 1,2,\ldots J\}$. The recursion relation for the polynomials is

$$u_{n+1}(\lambda) = (\lambda - B_n)u_n(\lambda) - \frac{h_n^2}{h_{n-1}^2}u_{n-1}(\lambda) \qquad \text{(B1)}$$

where the norms h_n are given by

$$h_n = \sum_{j=1}^{J} u_n^2(\lambda_j) \qquad \text{(B2)}$$

and the recursion constants B_n are given by

$$B_n = \frac{1}{h_n^2}\sum_{j=1}^{J} \lambda_j u_n(\lambda_j) \qquad \text{(B3)}$$

For example, the polynomials generated by this algorithm may be used to represent the latitude variations of the Fourier coefficients a_{mp} and b_{mp} used in the high-latitude representation:

$$a_{mp}(\lambda_j, \tau_l) = \sum_{n=1}^{N} \alpha_{mnp}(\tau_l) u_n(\lambda_j) \qquad \text{(B4)}$$

$$b_{mp}(\lambda_j, \tau_l) = \sum_{n=1}^{N} \beta_{mnp}(\tau_l) u_n(\lambda_j) \qquad \text{(B5)}$$

where

$$\alpha_{mnp}(\tau_l) = \frac{1}{h_n^2}\sum_{j=1}^{J} a_{mp}(\lambda_j, \tau_l) u_n(\lambda_j) \qquad \text{(B6)}$$

$$\beta_{mnp}(\tau_l) = \frac{1}{h_n^2}\sum_{j=1}^{J} b_{mp}(\lambda_j, \tau_l) u_n(\lambda_j) \qquad \text{(B7)}$$

Acknowledgments. Much of the development of PIM and PRISM was supported by the Geophysics Directorate of Phillips Laboratory through contracts with Computational Physics, Inc. (F19628-92-C-0044) and Boston University (F19628-K-90-0014).

References

Anderson, D. N., A theoretical study of the ionospheric *F*-region equatorial anomaly, II, Results in the American and Asian sectors, *Planet. Space. Sci.*, *21*, 421-442, 1973.

Bailey, G. J., and R. Sellek, A mathematical model of the Earth's plasmasphere and its application in a study of He^+ at L = 3, *Ann. Geophys.*, *8*, 171, 1990.

Beckmann, P., *Orthogonal Polynomials for Engineers and Physicists*, pp. 91092, Golem Press, Boulder, Colo., 1973.

Brace, L. H., and R. F. Theis, Global empirical models of ionospheric electron temperature in the upper F-region and plasmasphere based on in situ measurements from the Atmosphere Explorer-C, ISIS 1, and ISIS 2 satellites, *J. Atmos. Terr. Phys.*, *43*, 1317, 1981.

Davis, R. E., Predictability of Sea Surface Temperature and Sea Level Pressure Anomalies Over the North Pacific Ocean, *J. Phys. Oceanogr.*, 6, 249, 1976.

Decker, D. T., C. E. Valladares, R. Sheehan, Su. Basu, D. N. Anderson, and R. A. Heelis, Modeling daytime *F* layer patches over Sondrestrom, *Radio Sci.*, *29*, 249-268, 1994.

Fejer, B. G., The equatorial ionospheric electric fields, a review, *J. Atmos. Terr. Phys.*, *43*, 377-386, 1981.

Fejer, B. G., E. R. de Paula, I. S. Batista, E. Bonelli, and R. F. Woodman, Equatorial *F* region vertical plasma drifts during solar maxima, *J. Geophys. Res.*, *94*, 12,049-12,054, 1989.

Fejer, B. G., E. R. de Paula, R. A. Heelis, and W. B. Hanson, Global equatorial ionospheric vertical plasma drifts measured by the AE-E satellite, *J. Geophys. Res.*, *100*, 5769-5776, 1995.

Fox, M. W., and L. F. McNamara, Improved world-wide maps of monthly median f_oF_2, *J. Atmos. Terr. Phys.*, *50*, 1077, 1988.

Hardy, D. A., M. S. Gussenhoven, R. R. Raistrick, and W. J. McNeil, Statistical and functional representations of the pattern of auroral energy flux, number flux, and conductivity, *J. Geophys. Res.*, *92*, 12,275-12,294, 1987.

Hedin, A. E., MSIS-86 Thermospheric Model, *J. Geophys. Res.*, *92*, 4649-4662, 1987.

Hedin, A. E., Empirical global model of upper thermosphere winds based on Atmospheric and Dynamics Explorer satellite data, *J. Geophys. Res.*, *93*, 9959-9978, 1988.

Hedin, A. E., M. J. Buonsanto, M. C. Codrescu, M.-L. Duboin, C. G. Fesen, M. E. Hagan, K. L. Miller, and D. P. Sipler, Solar activity variations in midlatitude thermospheric meridional winds, *J. Geophys. Res.*, *99*, 17,601-17,608, 1994.

Heppner, J. P., and N. C. Maynard, Empirical high-latitude electric field models, *J. Geophys. Res.*, *92*, 4467-4489, 1987.

Hildebrand, F. B., *Methods of Applied Mathematics*, pp. 30-34, Prentice-Hall, Englewood Cliffs, N. J., 1965.

International Radio Consultative Committee (CCIR), CCIR atlas of ionospheric characteristics, *Rep. 340-4*, Int. Telecommun. Union, Geneva, 1967.

Jasperse, J. R., The photoelectron distribution function in the terrestrial ionosphere, in *Physics of Space Plasmas*, edited by T. S. Chang, B. Coppi, and J. R. Jasperse, pp. 53-84, Sci. Publ., Cambridge, Mass., 1982.

Klobuchar, J. A., and P. H. Doherty, The correlation of daily solar flux values with total electron content, paper presented at the International Beacon Satellite Symposium, Plasma Fusion Center, Mass. Inst. of Technol., Cambridge, July 6-10, 1992.

Kutzbach, J. E., Empirical eigenvectors of sea-level pressure, surface temperature, and precipitation complexes over North America, *J. Appl. Meteorol.*, *6*, 791, 1967.

Lorenz, E. N., *Empirical orthogonal functions and statistical weather prediction*, Sci. Rep. 1, Contract AF19(604)1566, AFCRC-TN-57-256, Dept. Meteorol., Mass. Inst. of Technol., Cambridge, 1956.

Moffett, R. J., The equatorial anomaly in the electron distribution of the terrestrial F-region, *Fundam. of Cosmic Phys.*, *4*, 313-391, 1979.

Peixota, J. P., and A. H. Oort, *Physics of Climate*, Appendix B, Am. Inst. of Phys., New York, 1991.

Preble, A. J., D. N. Anderson, B. G. Fejer, and P. H. Doherty, Comparison between calculated and observed *F* region electron density profiles at Jicamarca, Peru, *Radio Sci.*, *29*, 857-866, 1994.

Rush, C. M., M. PoKempner, D. N. Anderson, F. G. Stewart, and J. Perry, Improving ionospheric maps using theoretically derived values of f_oF_2, *Radio Sci.*, *18*, 95, 1983.

Rush, C. M., M. PoKempner, D. N. Anderson, J. Perry, F. G. Stewart, and R. Reasoner, Maps of f_oF_2 derived from observations and theoretical data, *Radio Sci.*, *19*, 1083, 1984.

Rush, C. M., M. Fox, D. Bilitza, K. Davies, L. McNamara, F. Stewart, and M. PoKempner, Ionospheric mapping: An update of f_oF_2 coefficients, *Telecommun. J.*, *56*, 179-182, 1989.

Schunk, R. W., A Mathematical Model of the Middle and High Latitude Ionosphere, *Pure Appl. Phys.*, *127*, 255-303, 1988.

Secan, J. A., and T. F. Tascione, The 4D Ionospheric Objective Analysis Model, paper presented at the 4th Ionospheric Effects Symposium, Naval Research Laboratory, Springfield, Va., May 1-3, 1984.

Sojka, J. J., R. W. Schunk, and W. F. Dennig, Ionospheric response to the sustained high geomagnetic activity during the March '89 great storm, *J. Geophys. Res.*, *99*, 21,341-21,352, 1994.

Strickland, D. J., D. L. Book, T. P. Coffey, and J. A. Fedder, Transport equation techniques for the deposition of auroral electrons, *J. Geophys. Res.*, *81*, 2755-2764, 1976.

Strickland, D. J., R. E. Daniell, J. R. Jasperse, and B. Basu, Transport-theoretic model for the electron-proton-hydrogen atom aurora, 2, Model results, *J. Geophys. Res.*, *98*, 21,533-21,548, 1993.

Strobel, D. F., and M. B. McElroy, The F2-layer at middle latitudes, *Planet. Space Sci.*, *18*, 1181, 1970.

D. N. Anderson, PL/GPIM, 29 Randolph Road, Hanscom AFB, MA 01731-3010. (e-mail: danderson@plh.af.mil)

L. D. Brown and R. E. Daniell, Jr., Computational Physics, Inc., Suite 202A, 240 Bear Hill Road, Waltham, MA 02154-1126. (e-mail: brown@plh.af.mil; daniell@plh.af.mil)

D. T. Decker and P. H Doherty, Institute for Space Research, Boston College, Chestnut Hill, MA 02159. (e-mail: decker@plh.af.mil; doherty@plh.af.mil)

M. W. Fox, Center for Space Physics, Boston University, Boston, MA 02215. (e-mail: matthewf@spica.bu.edu)

R. W. Schunk and J. J. Sojka, Center for Atmospheric and Space Science, Utah State University, Logan UT 84322-4405.

(Received May 4, 1994; revised June 7, 1994;
accepted June 14, 1995.)